EJNMMI Physics

ORIGINAL RESEARCH Open Access

Feasibility of a deep-inspiration breath-hold [^{18}F]AlF-NOTA-LM3 PET/CT imaging on upper-abdominal lesions in NET patients: in comparison with respiratory-gated PET/CT

Haiqiong Zhang[1], Meixi Liu[1], Ximin Shi[1], Jiangyu Ma[1], Chao Ren[1], Zhenghai Huang[1], Ying Wang[2], Hongli Jing[1] and Li Huo[1*]

*Correspondence:
Li Huo
huoli@pumch.cn
[1]Department of Nuclear Medicine, State Key Laboratory of Complex Severe and Rare Diseases, Beijing Key Laboratory of Molecular Targeted Diagnosis and Therapy in Nuclear Medicine, Peking Union Medical College Hospital, Chinese Academy of Medical Sciences, Beijing 100730, China
[2]Central Research Institute, United Imaging Healthcare, Shanghai 201815, China

Abstract

Purposes To explore the clinical feasibility and efficacy of a deep inspiration breath-hold (BH) PET/CT using [^{18}F]AlF-NOTA-LM3 on upper abdominal lesions in patients with neuroendocrine tumors (NETs).

Methods Twenty-three patients underwent a free-breath (FB) whole-body PET/CT, including a 10 min/bed scan for the upper abdomen with a vital signal monitoring for respiratory gating (RG) followed by a 20-second BH PET/CT covering the same axial range. For the upper abdomen bed, the following PET series was reconstructed: a 2-min FB PET; RG PET (6 bins); a 20-second and 15-second BH PET (BH_15 and BH_20). Semi-quantitative analysis was performed to compare liver SUV_{mean}, lesion SUV_{max}, MTV, its percentage difference and target-to-background ratio (TBR) between both BH PET and RG PET images. Subgroup analysis considered lesion location, MTV and SUV_{max}. A 5-point Likert scale was used to perform visual analysis and any missed or additional lesions were identified compared with RG PET.

Results Quantitative analysis on overall lesions ($n=78$) revealed higher SUV_{max} and TBR, and smaller MTV for both BH PET compared to FB and RG PET, with lesion location-specific variations. Neither significant difference was observed in all metrics between RG and FB PET in larger lesions, nor in MTV in lower-uptake lesions. However, both BH PET significantly enhanced these measurements. In the visual analysis, both BH PET showed noninferior performance to RG PET, and were evaluated clinically acceptable. Additional and missed lesions were observed in FB and both BH PET compared with RG PET, but didn't alter the clinical management. The BH_15 PET showed comparable performance to BH_20 PET in any comparison.

Conclusion The BH PET/CT using [^{18}F]AlF-NOTA-LM3 is effective in detecting upper abdominal lesions, offering more accurate quantitative measurements. Using a novel PET/CT scanner, a 15-second BH PET can provide comparable and superior performance to RG PET, indicating potential feasibility in clinical routines.

Keywords Deep-inspiration breath-hold, Respiratory gating, Free-breath, Neuroendocrine tumors

Introduction

Positron emission tomography/computed tomography (PET/CT) is a widely-used imaging modality for various aspects of cancer imaging, including (re)staging, therapy response monitoring, and suspected recurrence evaluation [1–4]. However, the quality of PET images can be compromised by motion, especially respiratory motion during acquisition, leading to image blurring, reduction in quantitative accuracy and a compromised reproducibility [5]. Moreover, in hybrid PET/CT imaging, this challenge becomes more significant due to the disparate respiration phases between PET and CT scans. The misalignment between PET and CT images can lead to mislocalization of lesions, and inaccurate standardize uptake value (SUV) measurements brought by errors in CT-based PET attenuation and scatter correction.

Numerous approaches have been developed to tackle motion artifacts in PET/CT imaging. Among these, respiratory gating (RG) technique has emerged as an effective method to mitigate respiratory motion effects during PET acquisition. This involves reconstructing PET data into bins based on amplitude or phase of the patient's breathing cycle. The technique depends on tracking the patient respiration signal from external motion detection system, such as pressure sensors, thermistors, spirometers, real-time video cameras, or data-driven [6–11]. To maintain a comparable image quality to that of clinical routines, the acquisition time for the gated bed is extended by a factor of four or higher, based on the gated bins (typically ranging from 4 to 10) during the reconstruction.

An alternative approach known as the deep-inspiration breath-hold (BH) PET technique has been proposed. BH methods have been reported to be effective in identifying anatomy and enhancing the accuracy of quantitative measurements [12–18]. Nevertheless, the studies faced the challenge of insufficient counts within a short acquisition which restricted the application of BH mainly in clinical routines. Over the past decades, there have been notable advancements in PET imaging technologies, including both hardware development such as scintillators, silicon photomultipliers, and application-specific integrated circuits (ASIC), as well as software development such as advanced reconstruction algorithms and post-processing techniques. Newly commercialized PET/CT systems, taking the advantages of these techniques, can provide enhanced spatial and temporal resolution along with high sensitivity. The superior timing resolution, facilitated by time-of-flight (TOF) technology, contributes to a multifold change in effective sensitivity, resulting in elevated image quality and contrast when compared to that of non-TOF PET scanners [19]. In our study, we utilized a novel PET/CT scanner (uMI Panorama, United Imaging Healthcare, China) with a system sensitivity of 20.1 kcps/MBq and a timing resolution of 189 ps [20], allowing for the exploration of a more feasible BH protocol for all patients. In previous studies, typical BH duration for single BH PET protocol was 20–30 s which is quite challenging [12–18]. In the study, we tried to reduce the acquisition time to 15 s and investigate its performance and diagnostic efficacy in clinical routines.

Neuroendocrine tumors (NETs) are a diverse group of tumors characterized by overexpression of somatostatin receptor (SSTR), which are present throughout the human body and most commonly found in the gastrointestinal tract, pancreas, and lungs [21, 22]. Utilizing a PET scan with a SSTR-targeted tracer allows for the visualization of NETs with high sensitivity, especially for upper abdominal lesions [23–25]. While the conventional tracers, ^{68}Ga-labeled somatostatin analogs, have shown impressive results, it is impeded by practical and economic challenges arising from the ^{68}Ge/^{68}Ga-generators. In contrast, ^{18}F-labeled SSTR-targeted PET tracers are of interest in research field recently and previous findings have indicated its promising efficacy in detecting NETs [26–30]. To our knowledge, there is a limited number of research investigating BH PET/CT imaging with ^{18}F-labeled SSTR-targeted tracers in abdominal lesions of NET patients. It is of significance to explore its utilization as an alternative to RG PET in clinical routines.

Thus, the aim of the study is to explore the feasibility and effectiveness of a 15-second and 20-second BH technique in upper-abdominal NETs in [^{18}F]AlF-NOTA-LM3 PET/CT imaging, in comparison with RG PET using both visual and semi-quantitative analysis.

Methods

Patients

Twenty-five patients, suspected of NETs or recurrence from Feb. 2023 to Jul. 2023, were prospectively included in this study. All patients were informed of the prolonged scan time and the procedure of breath hold during the scan. The enrolled patients were diagnosed with NETs which was confirmed by contrast-enhanced CT, and/or enhanced MR and/or follow-up results. Exclusion criteria includes: patients who were unable to lie still with a spine position, or for the prolonged duration of the scan; the scanned bed position for RG or BH was not suitable for an upper abdominal study.

The institutional review board of Peking Union Medical College Hospital approved our study; the written informed consent was signed by all patients prior to the examination.

Imaging protocol

All PET/CT imaging was performed using a SiPM- and ASIC-based PET/CT system (uMI Panorama, United Imaging Healthcare, Shanghai, China) with an axial field-of-view (FOV) of 35 cm and a timing resolution of 189 ps [20]. [^{18}F]AlF-NOTA-LM3 was synthesized by our lab. Patients were injected intravenously with 262±47 MBq of an [^{18}F]AlF-NOTA-LM3 and imaged 60 min later. Before patient positioning, a wireless vital signal monitoring (VSM) system supplied by the vendor was mounted to patients. A standard CT scan was obtained from the vertex to mid-thigh to provide attenuation correction information to PET and anatomical information to localize the lesions. The parameters of the standard CT were as follows: a fixed tube voltage of 120 kV, an auto-mAs technique for dose modulation, pitch factor of 0.9625 and 0.5-second gantry rotation time. Subsequently, a whole-body PET were obtained in 10 min for the bed covering upper abdominal region to generate RG PET images and 2 min per bed position for other regions. All the above-mentioned scans were acquired during free breathing without voice instruction. Immediately after the FB acquisition, a hybrid breath-hold PET/CT was acquired without any change of the patient position. Patients were instructed to hold his/her breathe in deep inspiration status during both CT and PET scans. A BH CT

was performed, followed by a 20-second BH PET acquisition of the same axial range as the RG PET. The acquisition protocol of BH CT was the same as the standard CT.

Both CT images were reconstructed using a soft tissue kernel for the vendor-provided standard iterative algorithm. The 10-min acquired data were rebinned to a 2-min non-gated PET (referred to as FB PET) data, which were used to represent the free breath PET in clinical routine. In addition, 6-bin gated images were generated from the 10-min data. BH PET images (referred to as BH_20 PET and BH_15 PET) were generated from the 20-second BH PET data. All PET data were reconstructed using ordered subset expectation maximization algorithm with the following parameters: 3 iterations, 10 subsets, FOV of 600 mm, matrix of 192×192, slice thickness of 2.9 mm, a Gaussian filter with full width half maximum of 4 mm. All PET reconstructions included the standard corrections like decay, scatter, random, dead time, attenuation, and normalization.

Image analysis

Image analyses were performed on a dedicated workstation (uWI, R002, United Imaging Healthcare, China). An experienced nuclear medicine physician (SXM, 10 years' experience) first reviewed the data, and decided the best-match bin of the RG PET images (referred to as RG PET) with the FB CT images, which were then split and used as a reference in this study.

Semi-quantitative analysis

In the semi-quantitative analysis, a volume of interest (VOI) with a diameter of 30±3 mm was manually drawn on a homogenous area of the right liver lobe for all PET series. The mean standardized uptake value (SUV) and standard deviation (SD) within the VOI were obtained, and coefficient of variation (COV) was calculated by dividing the SD by the SUV_{mean}. The physician reviewed RG PET images and randomly selected lesions in the upper abdomen (up to 5 per patient) and identified the corresponding ones in the FB and BH PET images. Lesions were measured using a 50% maximum SUV (SUV_{max}) threshold, and SUV_{max} and metabolic tumor volume (MTV) of the target lesions were obtained. If the lesion was not successfully segmented, a small ellipsoid VOI encompassing the lesion will be used to record the SUV_{max}. Target-to-background ratio (TBR) were calculated as a measure to indicate the lesion contrast. The percentage difference to FB PET of RG and BH PET was calculated and compared (referred to as %SUV-RG, %SUV-BH15, %SUV-BH20, and % MTV-RG, % MTV-BH15, % MTV-BH20.

). For each identified lesion, the location was categorized as organ-based (liver, pancreas, etc.) or metastatic lymph nodes. Subgroup analysis was performed based on the lesion location, size and uptake.

Visual analysis

Two nuclear medicine physicians (LMX and MJY, both 5 years' experience) performed visual assessment independently with a randomized reading order of the PET series for each patient. The patient clinical information, the acquisition and reconstruction information were blinded to the readers. Both the physicians viewed PET and corresponding CT images and assessed the image quality using a 5-point Likert scale in the following three perspectives: motion artifact, diagnostic confidence, and PET and CT alignment (with 1=best and 5=worst). Images with a score of 3 and below were clinically

acceptable. In case of discrepancy between readers, decisions were made by the above-mentioned experienced nuclear medicine physician (SXM, 10 years' experience). In a subsequent week following the analysis, the three nuclear medicine physicians reviewed all images in comparison with RG PET in a joint session and identified any additional lesions, missed lesions, and changes in clinical management.

Statistical analysis

Continuous data are presented as the mean ± SD and range. All statistical analysis was performed using SPSS Statistics, version 27 (IBM, Armonk, NY, USA). All the parameters in the semi-quantitative analysis were tested for normality using the Kolmogorov-Smirnov test and the two-tailed paired *t*-test was subsequently performed. Bonferroni correction was applied for the multiple comparisons. Cohen's kappa test was used to evaluate inter-reader agreement. The scores in the visual analysis were subsequently compared using the Wilcoxon signed-rank test. A p-value of less than 0.05 was considered statistically significant.

Results

A total of 23 patients (female/male: 8/15, age: 25–75 years) were finally included in the study with two excluded participants. The demographic and clinical information of the enrolled patients are listed in Table 1. Among them, 4 patients were scanned for initial diagnosis or staging, 6 patients were for treatment monitoring, and the remained 13 patients were for recurrence detection.

Table 1 Patient demographic characteristics

Parameter	Value
Age (years)	54.1 ± 11.7 [25, 75]
Weight (kg)	64.9 ± 8.9 [49, 80]
Height (cm)	167.5 ± 6.3 [155, 178]
Gender	
Female	8 [+]
Male	15 [+]
BMI	23.1 ± 2.9 [17.7, 28.3]
Injected activity (MBq)	262 ± 47 [185, 335]
Uptake time (min)	91 ± 23 [62, 155]
Primary cancer type	
Duodenum NET	1[+]
Gastric NET	1[+]
Ileocecal NET	1[+]
Jejunum NET	1[+]
Lung NET	1[+]
MEN	1[+]
Pheochromocytoma	1[+]
Pancreatic NET	10[+]
Rectum NET	3[+]
Small intestinal NET	1[+]
Thyroid NET	1[+]
Unknown origin	1[+]

Data are presented as the mean ± standard deviation [minimum, maximum]

[+] Number of patients

BMI, body mass index; NET, neuroendocrine tumour; MEN, multiple endocrine neoplasia

Semi quantitative analysis

In the semi-quantitative analysis, the uptake and noise in the liver were first analyzed. The SUV_{mean} of liver in FB, BH_15 and BH_20 PET demonstrated good agreement with RG PET, indicating a high level of accuracy in PET quantification, as illustrated in Fig. 1. In comparison to FB PET, the image quality of RG, BH_15 and BH_20 PET was significantly degraded with a reduced COV value ($p<0.05$, $p<0.001$, and $p<0.001$, respectively). This image quality degradation was primarily attributed to the limited counts acquired from the short time. Subsequently, the clinical acceptability of these PET images was assessed through visual analysis.

A total of 78 lesions were included in the analysis, and two out of 78 lesions were unsuccessfully segmented and recorded only with SUV_{max} information. The lesion SUV_{max} in RG, BH_15 and BH_20 PET were all found significantly higher than that in FB PET ($p<0.01$, $p<0.001$, and $p<0.001$, respectively), as illustrated in Fig. 2A. Furthermore, both the BH groups showed significantly increased lesion SUV_{max} compared to RG PET, suggesting superior capability in elevating the lesion SUV measurements ($p<0.001$). Nevertheless, no significant difference was observed between both BH PET images ($p=1.0$). In addition, %SUV-BH15 and %SUV-BH20 proved significantly higher than %SUV-RG, indicating a more robust capability in recovering SUV measurements (both $p<0.001$, Fig. 2B). Notably, there was no significant difference between %SUV-BH15 and %SUV-BH20 ($p=1.0$). Figure 3 illustrates PET images of a 25-year-old female patient diagnosed with pancreatic NET (G1) with bone and liver metastases. As observed in the MIP images (upper row), lesions in the upper abdomen in FB PET are blurred with severe distortion, while these distortion can be well recovered in RG and both BH PET images. In the bottom row, RG PET and both BH PET can better image the lesions compared to FB PET as indicated with a red hollow arrow. In addition, an increase in the lesion SUV_{max} was found as 13.04 for FB PET, 19.75 for RG PET, 25.85 for BH_15 PET, and 25.09 for BH_20 PET.

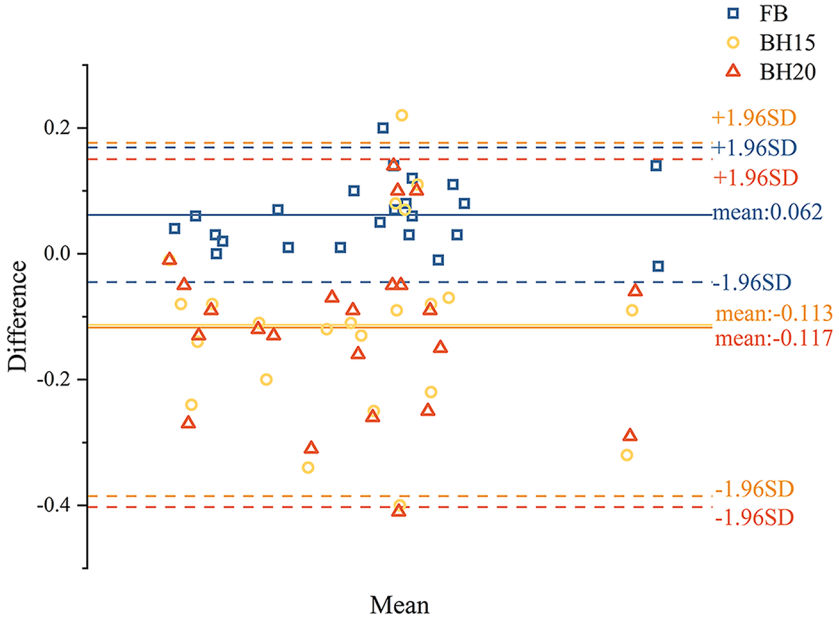

Fig. 1 Bland-Altman plots of liver SUV_{mean} in FB, BH_15, and BH_20 PET showed good agreement with that in RG PET

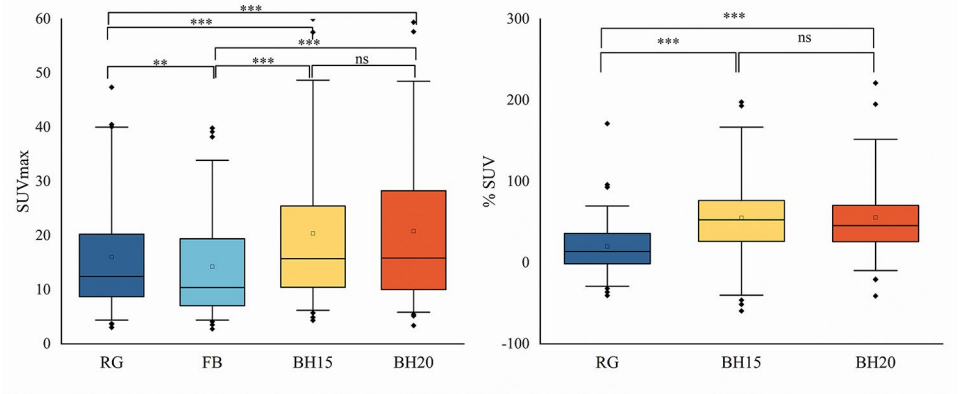

Fig. 2 Boxplots of (**A**) lesion SUV_{max} and (**B**) percentage difference of lesion SUV_{max} (%SUV) compared to the FB PET. Compared to FB PET, lesion SUV_{max} in RG, BH_15 and BH_20 groups was significantly higher. The percentage difference of lesion SUV_{max} in BH groups also showed significantly difference compared to RG group. However, there was no significant difference in lesion SUV_{max} and percentage difference of lesion SUV_{max} between BH groups. SUV_{max}, the maximum of standardized uptake value; %SUV, percentage difference in lesion SUV_{max} compared to FB PET; * $p<0.05$; ** $p<0.01$; *** $p<0.001$; ns, no significant difference

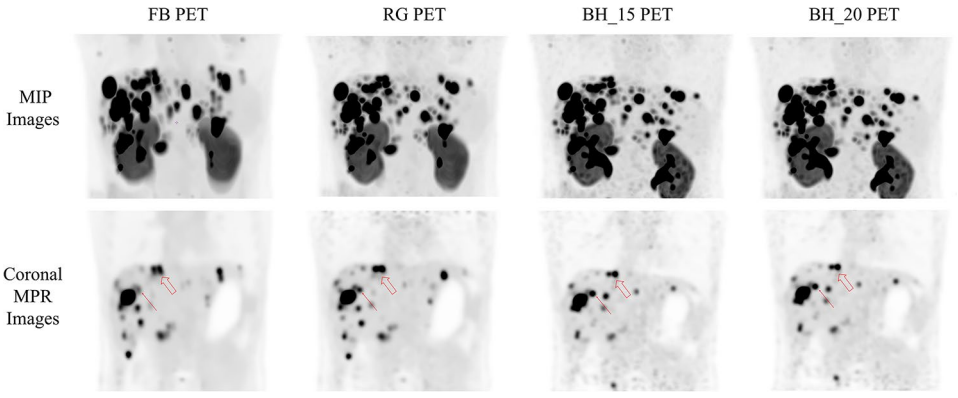

Fig. 3 PET images of a 25-year-old female patients diagnosed with pancreatic NET (G1) with liver and bone metastases. Severe distortion of lesions can be observed in both MIP and MPR images in FB PET, while these distortion can be well recovered in RG and both BH PET. NET, neuroendocrine tumor; MIP, maximum intensity projection; MPR, multi planar reconstruction; RG, respiratory gating; BH, breath hold

To investigate image contrast and lesion conspicuity, we employed TBR as a metric and observed a significant elevation in TBR values for RG, BH_15 and BH_20 PET compared to FB PET (all $p<0.001$, Fig. 4). There was a significant enhanced image contrast in both BH PET images compared with RG PET images (both $p<0.001$), and no significance was found between both BH PET images ($p=1.0$).

With regard to MTV, the mean of RG PET exhibited a comparable value with that in FB PET without significant difference ($p=0.094$), but higher than those in both BH PET (both $p<0.001$), as illustrated in Fig. 5A. Likewise, the MTV between both BH PET images was not significantly different ($p=0.750$, Fig. 5A). Regarding the percentage difference in MTV, we found that both BH PET had a significantly lower value than that in RG PET (both $p<0.001$, Fig. 5B), indicating their capacity of BH PET to further reduce the MTV compared to RG PET. Notably, there was no significant difference in the percentage difference in MTV between both BH PET ($p=1.0$).

In the subgroup analysis categorized by the tumor location, we observed varying statistical significances in liver tumors ($n=60$), pancreatic tumors ($n=6$) and lymph nodes

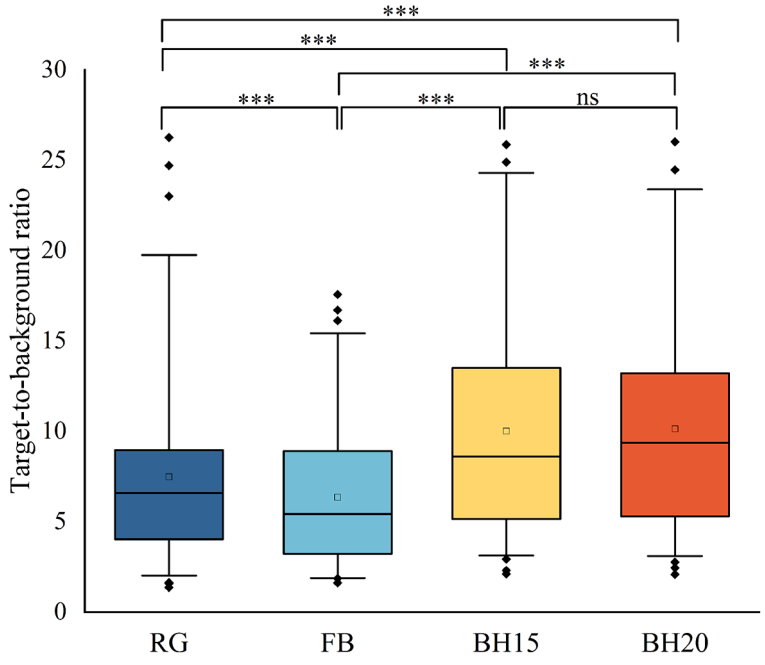

Fig. 4 Comparison of TBR between FB, RG, BH_15 and BH_20 PET. Compared with FB PET, the TBR in RG, BH_15 and BH_20 PET were significantly higher, indicating a higher image contrast and a better lesion conspicuity. BH PET groups further showed a significantly higher TBR than that in RG PET, but no significance was found between both BH PET groups. TBR, target-to-background ratio; *** $p < 0.001$; ns, no significant difference

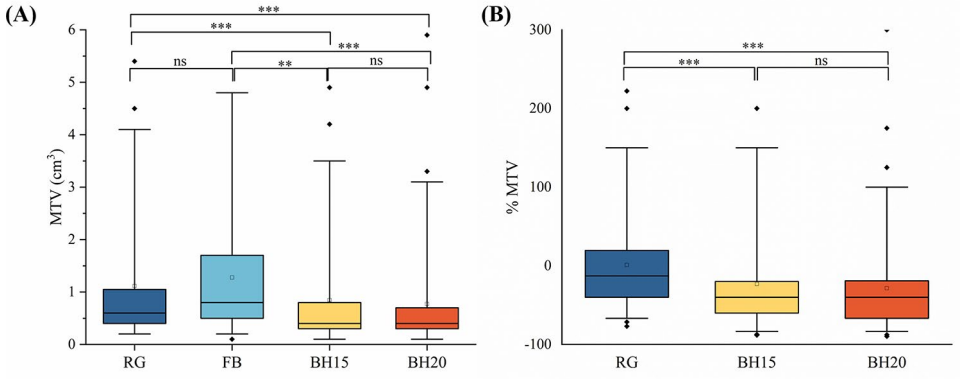

Fig. 5 Boxplots of (**A**) lesion MTV and (**B**) percentage difference in MTV compared to FB PET. RG, BH_15 and BH_20 PET showed a significantly lower MTV than that in FB PET. Both BH PET had significantly reduced MTV compared to RG PET, and no significance was found between BH groups. MTV, metabolic tumor volume; %MTV, percentage difference in MTV compared to FB PET; ** $p < 0.01$; *** $p < 0.001$; ns, no significant difference; RG, respiratory gating; BH, breath hold

($n=8$). Regarding the lesion SUV_{max}, both BH PET showed significantly increase compared to RG and FB PET in liver and pancreatic tumors (all $p<0.05$), but no significant difference in lymph nodes ($p=1.0$ for BH_15 and BH_20, Fig. 6). In addition, compared to FB PET, RG PET only significantly enhanced the SUV_{max} measurement in liver tumors ($p<0.01$), but no statistical difference was found in pancreatic tumors and lymph nodes (both $p=1.0$). In the analysis of MTV, there were significant differences between both BH PET and RG PET images in liver tumors (both $p<0.001$), but no significant differences in pancreatic tumors ($p=0.650$ and 0.630) and lymph nodes (both $p=1.0$). However, both BH PET significantly reduced MTV compared to FB PET in liver tumors

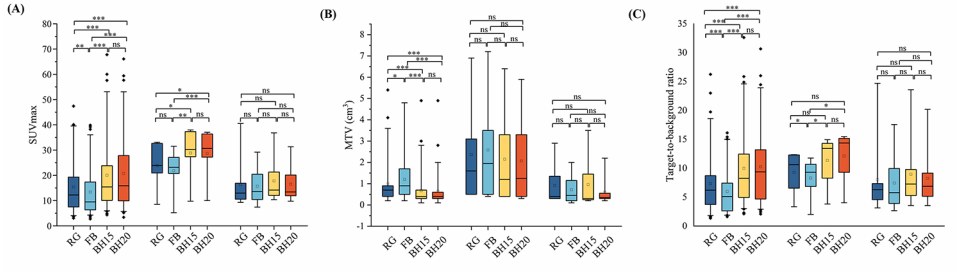

Fig. 6 Subgroup analysis of (**A**) lesion SUV_{max}, (**B**) MTV, and (**C**) target-to-background ratio (left: liver; middle: pancreas; right: lymph node) for different tumor location. Differences in statistical significance can be found in different tumor locations. SUV_{max}, the maximum of standardized uptake value; MTV, metabolic tumor volume; * $p<0.05$; ** $p<0.01$; *** $p<0.001$; ns, no significant difference; RG, respiratory gating; BH, breath hold

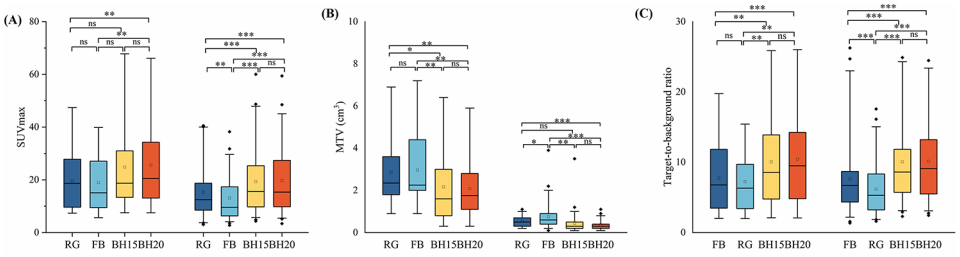

Fig. 7 Subgroup analysis of (**A**) lesion SUV_{max}, (**B**) MTV, and (**C**) target-to-background ratio (left: lesions with large volume; right: lesions for small volume) for different lesion volume. Compared to FB PET, both BH PET can significantly increase lesion SUV_{max}, TBR while reduce MTV in both groups. There was no significant difference in the three metrics between both BH PET images. SUV_{max}, the maximum of standardized uptake value; MTV, metabolic tumor volume; * $p<0.05$; ** $p<0.01$; *** $p<0.001$; ns, no significant difference; RG, respiratory gating; BH, breath hold

(both $p<0.001$), but still showed comparable measurements in pancreatic tumors and lymph nodes (both $p=1.0$). With regard to TBR, RG PET and both BH PET showed significantly improved measurements compared to FB PET in liver (all $p<0.001$) and pancreatic tumors (all $p<0.05$), but not in lymph nodes. Notably, no significant difference was observed between both BH PET images in the above analysis.

The subsequent subgroup analysis was performed based on the tumor size, with all included lesions categorized into two groups with a cutoff value of 1.0 cm^3: a large lesion group (L-group) and a small lesion group (S-group) measured in RG PET images. In the L-group ($n=18$), no significant difference was observed in lesion SUV_{max}, MTV and TBR between FB and RG PET (all $p=1.0$), suggesting a limited effectiveness of the RG technique in larger lesions (Fig. 7). However, SUV_{max} in BH_20 PET was significantly higher ($p<0.01$) while lesion SUV_{max} in BH_15 PET was slightly elevated; MTV was significantly reduced (both $p<0.01$); and the TBR was significantly improved ($p<0.01$, and <0.001, respectively), compared to FB PET. This implies RG PET yielded comparable quantitative measurements to FB PET in lesions with larger volumes, while both BH PET showed significant or slight enhancement in these measurements. Conversely, in the S-group ($n=58$), MTV in RG and both BH PET were significantly lower than that in FB PET ($p<0.05$, 0.01 and 0.001, respectively), while SUV_{max} were significantly elevated ($p<0.01$, 0.001 and 0.001, respectively). Consequently, TBR in RG and both BH PET showed a significant improvement compared to FB PET (all $p<0.001$). Moreover, in these two subgroups, no significant difference was found in SUV_{max}, MTV and

TBR between both BH PET groups, indicating comparable quantitative measurements regardless of tumor size (L-group: $p=0.462$, 0.395, and 0.356; S-group: $p=0.483$, 0.265 and 0.736, respectively).

Lesion uptake served as another criteria for categorizing lesions into two subgroups: a high uptake group (HU-group) and a low uptake group (LU-group), using a cutoff value of 16.3 measured in RG PET images. In the HU-group ($n=32$), both BH PET exhibited a significantly higher SUV_{max} and lower MTV compared with FB PET (all $p<0.05$), as illustrated in Fig. 8. However, RG PET showed comparable SUV and MTV with FB PET (both $p=1.0$). The TBR in RG PET was significantly higher than in FB PET ($p<0.05$), and lower than in both BH PET (both $p<0.001$). No statistical significance was found in SUV_{max}, MTV and TBR between both BH groups. In contrast, in the LU-group low uptake group ($n=46$), there was a significant difference in SUV_{max} and TBR between RG and FB PET ($p<0.01$, and 0.001, respectively), but no difference in MTV. However, both BH groups exhibited a significantly higher SUV_{max} (both $p<0.001$), lower MTV (both $p<0.01$), and higher TBR (both $p<0.001$) compared to FB PET. Similarly, no statistical significance was found in these three metrics between both BH groups (all $p=1.0$).

Visual analysis

The overall inter-reader agreement in the visual analysis demonstrated a Cohen's kappa of 0.719, representing a substantial agreement. The mean scores±SD for FB, RG, BH_15, and BH_20 PET were as follows: for respiratory motion artifacts, 2.61±1.16, 1.61±0.72, 1.17±0.39, and 1.13±0.34; for overall diagnostic confidence, 1.56±0.73, 1.09±0.29, 1.13±0.34, and 1.04±0.21; and for PET and CT alignment, 1.87±0.81, 1.87±0.76, 1.52±0.66, and 1.65±0.78. Regarding the respiratory motion artifacts, RG and both BH PET exhibited significantly fewer artifacts compared to FB PET ($p<0.01$, 0.001, and 0.001, respectively), as illustrated in Fig. 9. Both BH PET showed significantly reduced respiratory motion artifacts compared to RG PET (both $p<0.05$), suggesting a superior performance of the BH approach in mitigating respiratory motion. No significant difference was observed between RG and both BH PET (both $p=1.0$) in terms of diagnostic confidence, indicating a comparable performance for clinical use. However, all of them showed significantly higher diagnostic confidence compared to FB PET (all $p<0.05$). As shown in Fig. 10, a high uptake lesion (arrow) was found in a patient with rectum NET for treatment monitoring and suspected of a metastatic lymph node or a metastasis of gastric antrum in routine FB PET/CT images. However, the diagnostic confidence can

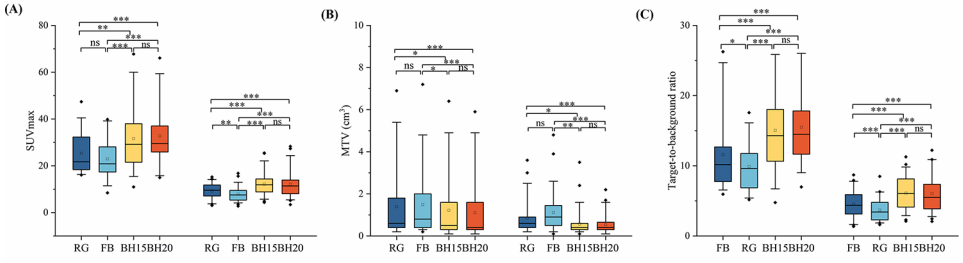

Fig. 8 Subgroup analysis of (**A**) lesion SUV_{max}, (**B**) MTV, and (**C**) target-to-background ratio (left: lesions with higher uptake; right: lesions for lower uptake) for different lesion SUV_{max}. BH PET can significantly increase lesion SUV_{max}, TBR while reduce MTV regardless of lesion SUV_{max}. There was no significant difference in the three metrics between both BH PET images. SUV_{max}, the maximum of standardized uptake value; MTV, metabolic tumor volume; * $p<0.05$; ** $p<0.01$; *** $p<0.001$; ns, no significant difference; RG, respiratory gating; BH, breath hold

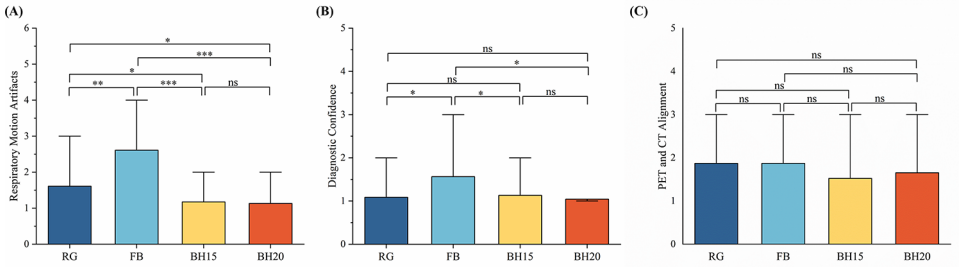

Fig. 9 Scores of visual analysis in the three perspectives: (**A**) respiratory motion artifacts; (**B**) diagnostic confidence; (**C**) PET and CT alignment. Regarding the respiratory motion artifacts and diagnostic confidence, BH PET exhibited significantly better performance than FB PET. However, there was no significant difference between FB, RG and both BH PET regarding the PET and CT alignment. ** $p < 0.01$; *** $p < 0.001$; ns, no significant difference; RG, respiratory gating; BH, breath hold

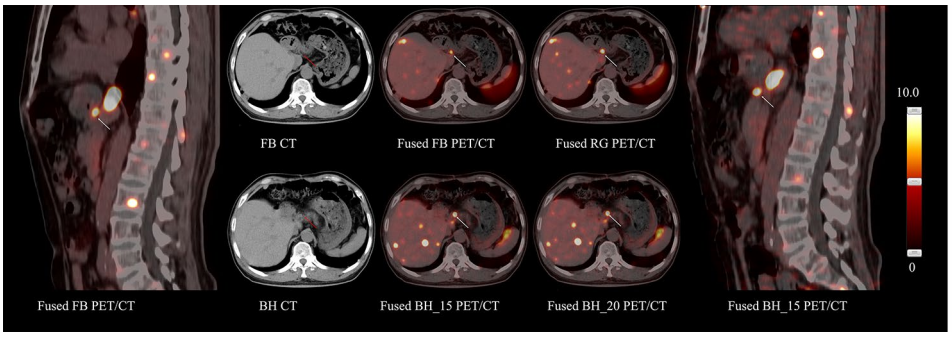

Fig. 10 PET/CT images of a 57-year-old male patient with rectum NET. The diagnostic confidence on the metastasis (arrow) was improved in BH PET/CT compared with FB PET/CT. NET, neuroendocrine tumor; MIP, maximum intensity projection; RG, respiratory gating; BH, breath hold

be improved in both BH PET/CT images. With regards to PET and CT alignment, no significant difference was observed between PET series. Likewise, there was no significant difference in the three perspectives between both BH PET images (p=1.0, 0.785, and 1.0, respectively).

We employed RG PET as a reference for evaluating lesion detectability. In a patient-base analysis, FB PET detected additional lesions (3/23) and both BH PET detected even additional lesions (10/23). Missed lesions were observed in both BH PET (3/23), while FB PET missed lesions in additional three patients (6/23 in total). Furthermore, we found that these additional findings and omissions didn't alter the clinical management in the present study due to the nature of multiple metastases in NETs.

Discussion

This study was designed to investigate the feasibility and effectiveness of a single deep-inspiration breath-hold acquisition in [^{18}F]AlF-NOTA-LM3 PET/CT imaging. The main findings are as follows: (a) BH PET acquisition provides more accurate quantitative measurements of SUV_{max} and MTV and enhanced contrast in upper abdominal lesions in comparison with conventional FB PET; (b) compared with RG PET, non-inferior results were found in BH PET regarding the semi-quantitative metrics in overall lesions analysis and subgroup analysis; additional and missed lesions were observed in BH PET but without necessity to change the clinical management; (c)the effectiveness of BH PET were found different in lesion location and volume compared to FB PET; (d) although

quality of BH PET images is generally inferior to that of RG PET and FB PET but they were evaluated clinically acceptable; (e) BH_15 PET showed comparable performance compared to BH_20 PET.

While RG technique is widely acknowledged in research, its applications in clinical routines is constrained. The limitation arises from the complexity in the setting of external device to capture respiratory signal and/or its prolonged scan time [7–11]. Therefore, it may pose challenges to the daily clinical workflow, especially in busy sites and departments. In contrast, the BH approach only requires an additional short acquisition of several seconds, resulting in minimal interruption to the clinical workflow. In previous studies, the typical duration of a single BH acquisition was 20 s. However, research has indicated that this duration may not be universally acceptable, particularly for certain patient populations such as older individuals and those with underlying lung diseases [18]. To explore a boarder feasibility, we utilized a novel PET/CT scanner with ultra-high sensitivity, presenting the potential to further reduce the acquisition time in a BH scan. In comparison with conventional BH_20 PET imaging, the BH_15 PET has demonstrated comparable semi-quantitative metrics and clinical acceptability, making it more feasible to a wider range of patients.

Gastrointestinal tract NETs are the most common type, and both primary and metastatic NETs are often found in the upper abdomen, where they are inevitably impacted by respiratory motion. Unlike the thorax, imaging tumors in the upper abdomen encounters difficulties due to the high uptake of normal background tissue in PET imaging. Respiratory motion can result in blurred lesions and reduced contrast between lesions and background, making it difficult to confidently identify lesions for diagnosis. In the CT part, lesions in these regions, such as those in the liver, are challenging or even impossible to be identified because their density are similar to that of the surrounding tissues. Therefore, when imaging NETs in the upper abdomen, efforts should be made to mitigate or eliminate the respiratory motion artifacts. Respiratory gating technique is well known for its effectiveness in minimizing the impact of respiratory motion in PET imaging. In a previous study, the use of a prospective data-driven respiratory gating (DDG-RG) acquisition with ^{68}Ga-DOTANOC in patients with NETs demonstrated superior results, showing increased lesion SUV and reduced lesion volume. However, certain patients did not fully benefit from the DDG technique due to software triggering requirements. Furthermore, the considerably prolonged scan time, up to 4 min per bed position, still posed disruptions to the workflow during subsequent patient preparation and presented notable challenges in clinical routines [31]. In contrast, the BH method is more straightforward, requiring only an additional fast acquisition. Thus, its negligible impact on daily workflow makes it feasible integrated in clinical routines.

In our study, the breath hold method has demonstrated the advantage of providing more accurate quantitative measurements in PET imaging in lines with other research. In the present study, the lesion SUV_{max} measured in BH_15 and BH_20 PET were up to 55.3% and 55.7% higher than those in FB PET. This increase can primarily be attributed to two factors: the longer uptake time for BH PET and the BH method which can eliminate the effects of respiratory motion. Since the interval between the FB and BH PET acquisitions was within 10 min, the impact of uptake time is minimized. Therefore, the observed difference in SUV can be largely attributed to respiratory motion. Such a SUV increase is more prominent in liver lesions (62.8% and 64.3%), and less in pancreatic

lesions (28.8% and 28.7%) and metastatic lymph nodes (19.2% and 14.0%). The increase in liver and pancreatic lesions is quite comparable to a previous study using ^{18}F-FDG PET/CT imaging [16]. The increase in lesion SUV_{max} also found more pronounced in lesions with small volume (60.4% and 61.1%) and less pronounced in large volume(37.2% and 37.6%), suggesting that small lesions are more vulnerable to the respiratory motion. In addition, in the analysis for lower- and higher-uptake lesions, similar result was found in the two subgroups regarding %SUV-BH15 and %SUV-BH20. With regard to MTV, the measurements in BH_15 and BH_20 PET were decreased to 77.1% and 71.9% of those in FB PET, in line with the findings using a BH or a RG technique [16, 17].

This research has demonstrated the diagnostic efficacy of a BH PET/CT imaging protocol in clinical settings. In the visual analysis of the present study, we found both BH PET can reduce the respiratory motion artifacts and provide adequate diagnostic confidence. Moreover, with the BH CT, the misalignment between CT and PET can be addressed, and the lesions can be better localized and characterized in both BH PET/CT images. Figure 11 illustrates PET/CT images of a 52-year-old male patients diagnosed with NET of unknown origin. In PET MIP and fused images, the liver mass in FB PET/CT, as indicated with an arrow, was noted in extrahepatic areas, but was more precisely localized in the BH PET/CT images. Nevertheless, we observed a discrepancy in the breathing phase during BH PET and CT acquisitions in 1 out of 23 patients. This discrepancy can primarily be attributed to inadequate training on the procedure of deep inspiration breath-hold. The study assumed that all patients could effectively sustain breath-hold for a minimum of 20 s based on the findings from previous studies. However, our observations revealed that a particular patient held her breath at various phases of the breathing cycle. Although 95.7% of the enrolled patients exhibited a successful BH acquisition, it is crucial to provide training on deep inspiration and breath-hold before the examination, especially when implementing this technique to elder patients in clinical routines. Another concern is that performing BH CT to match the BH PET

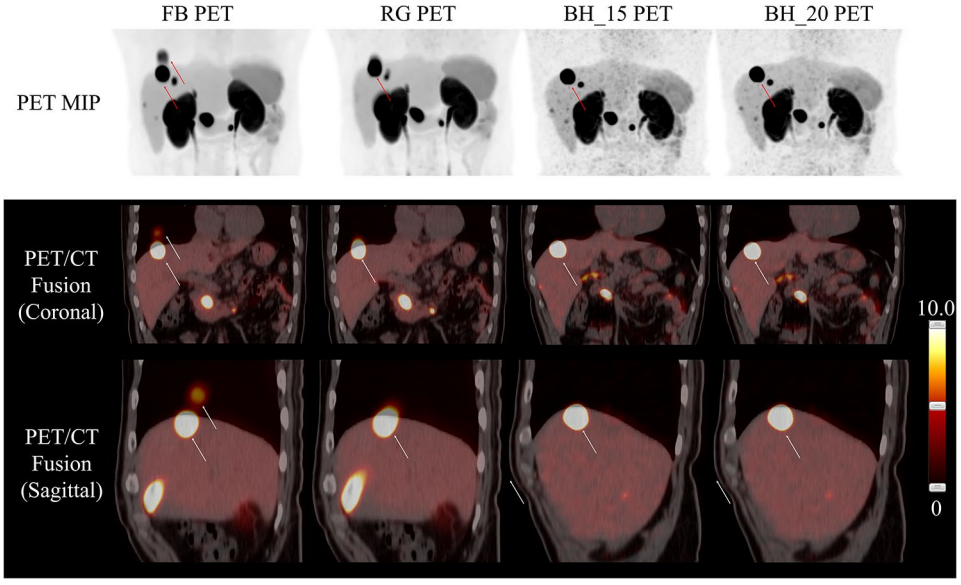

Fig. 11 PET/CT images of a 52-year-old male patient diagnosed with NET (G2) of unknown origin. Due to the respiratory motion, the liver mass (arrow) exceeded the hepatic dome in the FB PET/CT images but was successfully corrected in the BH PET/CT images. NET, neuroendocrine tumor; MIP, maximum intensity projection; RG, respiratory gating; BH, breath hold

might introduce additional radiation exposure to patients. Therefore, it is essential to implement training procedures to maximize the success rate of BH acquisition. Meanwhile, we found that 1 out of 23 patients had a shallow and irregular breathing pattern during PET acquisition, resulting in the clinically unacceptable quality of the RG PET images. However, it was noted that this particular patient could effectively cooperate with the breath-hold acquisition. It is known that one of the limitations of the RG technique, regardless of amplitude-based or phase-based, is its insufficient ability to handle such irregular breathing patterns. Thus, for these patients, BH acquisition can serve as an alternative to RG PET. Compared with RG PET, the reference in our study, additional lesions have been identified in BH PET. RG technique has been proved useful in mitigating the respiratory motion artifacts, but can't work effectively for all individuals. This attributes to the intrinsic limitation of the technique which relies on amplitude of the respiratory signal. As observed in our department, the performance of RG imaging on individuals with an asthenic habitus is suboptimal due to their shallow respiratory amplitude. Due to the increased image noise, lesions were also missed in both BH PET. All these findings didn't alter the clinical management because multiple metastases are commonly found in NETs.

One of the limitations in the present study is the relatively small number of the enrolled subjects using a single radiopharmaceutical. To address this limitation, a large-scale investigation should be performed with more extensive patient cohort and various radiopharmaceuticals. Additionally, incorporating additional training on patient breath is advisable. Another limitation in our study is the lack of pathologic confirmation of the additional identified lesions. While the decision was made by the experienced nuclear medicine physicians, the accuracy of the diagnosis needs validation in future study. Thirdly, although the acquisition times and protocols were anonymized, physicians could still identify the BH PET images due to their relatively higher noise levels. As a result, there may have been bias when physicians rated the images during the visual analysis. Finally, the reconstruction parameters in BH PET were selected based on our experience and were not optimized. We propose that optimizing these reconstruction parameters in BH PET could potentially enhance its performance and feasibility.

Conclusion

The deep-inspiration breath-hold PET/CT acquisition is effective in [^{18}F]AlF-NOTA-LM3 imaging in NET patients with upper abdominal lesions as it can provide more accurate quantitative measurements. Using a novel PET/CT scanner, a 15-second BH PET imaging can provide comparable and better performance to the RG imaging, suggesting its feasibility to provide complementary information to the routine FB PET/CT imaging.

Acknowledgements

We are very grateful to Lei Shi from United Imaging Healthcare for their assistance in the protocol design.

Author contributions

Study conception and design: Haiqiong Zhang, Meixi Liu, and Li Huo; Material preparation and data collection: Haiqiong Zhang, Ximin Shi, Jiangyu Ma, Chao Ren, Zhenghai Huang and Ying Wang; Data analysis: Haiqiong Zhang, Meixi Liu; Drafting of the manuscript: Haiqiong Zhang, Meixi Liu and Hongli Jing; All authors commented on previous versions of the manuscript and read and approved the final manuscript.

Funding

This work was sponsored in part by CAMS innovation fund for medical science (No. CIFMS-2022-I2M-JB-001, CIFMS-2021-I2M-1-025, CIFMS-2021-I2M-1-002, CIFMS-2021-I2M-1-003); National Key Research and Development Program of China

(No. 2016YFC0901500); National High Level Hospital Clinical Research Funding (XH-QN-012 K, 2022-PUMCH-D-001, 2022-PUMCH-B-071, 2022-PUMCH-C-037).

Data availability
Data are available on request to the corresponding author.

Code availability
Not applicable.

Declarations

Ethical approval
The study was approved by The Ethics Committee of Peking Union Medical College Hospital (I-23PJ312). All procedures performed in studies involving human participants were in accordance with the 1964 Helsinki declaration and its later amendments or comparable ethical standards.

Consent to participate
All participants signed the informed consent prior to the study.

Consent for publication
Patients signed informed consent regarding publishing their data and photographs for scientific use.

Conflict of interest
All authors have no conflicts of interest to report.

Received: 14 April 2024 / Accepted: 5 August 2024
Published online: 29 August 2024

References

1. Groheux D. FDG-PET/CT for primary staging and detection of recurrence of breast Cancer. Semin Nucl Med. 2022;52(5):508–19. https://doi.org/10.1053/j.semnuclmed.2022.05.001.
2. Groheux D, Cochet A, Humbert O, Alberini JL, Hindié E, Mankoff D. ^{18}F-FDG PET/CT for staging and restaging of breast Cancer. J Nucl Med. 2016;57(Suppl 1):S17–26. https://doi.org/10.2967/jnumed.115.157859.
3. El-Galaly TC, Villa D, Gormsen LC, Baech J, Lo A, Cheah CY. FDG-PET/CT in the management of lymphomas: current status and future directions. J Intern Med. 2018;284(4):358–76. https://doi.org/10.1111/joim.12813.
4. Sheikhbahaei S, Verde F, Hales RK, Rowe SP, Solnes LB. Imaging in Therapy Response Assessment and Surveillance of Lung Cancer: evidenced-based Review with Focus on the utility of 18F-FDG PET/CT. Clin Lung Cancer. 2020;21(6):485–97. https://doi.org/10.1016/j.cllc.2020.06.020.
5. Nehmeh SA, Erdi YE. Respiratory motion in positron emission tomography/computed tomography: a review. Semin Nucl Med. 2008;38(3):167–76. https://doi.org/10.1053/j.semnuclmed.2008.01.002.
6. van Elmpt W, Hamill J, Jones J, De Ruysscher D, Lambin P, Ollers M. Optimal gating compared to 3D and 4D PET reconstruction for characterization of lung tumours. Eur J Nucl Med Mol Imaging. 2011;38(5):843–55. https://doi.org/10.1007/s00259-010-1716-6.
7. Van Der Gucht A, Serrano B, Hugonnet F, Paulmier B, Garnier N, Faraggi M. Impact of a new respiratory amplitude-based gating technique in evaluation of upper abdominal PET lesions. Eur J Radiol. 2014;83(3):509–15. https://doi.org/10.1016/j.ejrad.2013.11.010.
8. Kang SY, Moon BS, Kim HO, Yoon HJ, Kim BS. The impact of data-driven respiratory gating in clinical F-18 FDG PET/CT: comparison of free breathing and deep-expiration breath-hold CT protocol. Ann Nucl Med. 2021;35(3):328–37. https://doi.org/10.1007/s12149-020-01574-4.
9. Guerra L, De Ponti E, Elisei F, et al. Respiratory gated PET/CT in a European multicentre retrospective study: added diagnostic value in detection and characterization of lung lesions. Eur J Nucl Med Mol Imaging. 2012;39(9):1381–90. https://doi.org/10.1007/s00259-012-2148-2.
10. Suzawa N, Ichikawa Y, Ishida M, Tomita Y, Nakayama R, Sakuma H. Respiratory-gated time-of-flight PET/CT during whole-body scan for lung lesions: feasibility in a routine clinical setting and quantitative analysis. Ann Nucl Med. 2016;30(10):722–30. https://doi.org/10.1007/s12149-016-1118-3.
11. Walker MD, Morgan AJ, Bradley KM, McGowan DR. Data-Driven Respiratory Gating outperforms device-based gating for clinical 18F-FDG PET/CT. J Nucl Med. 2020;61(11):1678–83. https://doi.org/10.2967/jnumed.120.242248.
12. Meirelles GS, Erdi YE, Nehmeh SA, et al. Deep-inspiration breath-hold PET/CT: clinical findings with a new technique for detection and characterization of thoracic lesions. J Nucl Med. 2007;48(5):712–9. https://doi.org/10.2967/jnumed.106.038034.
13. Kawano T, Ohtake E, Inoue T. Deep-inspiration breath-hold PET/CT versus free breathing PET/CT and respiratory gating PET for reference: evaluation in 95 patients with lung cancer. Ann Nucl Med. 2011;25(2):109–16. https://doi.org/10.1007/s12149-010-0442-2.
14. Balamoutoff N, Serrano B, Hugonnet F, Garnier N, Paulmier B, Faraggi M. Added Value of a single fast 20-second deep-inspiration breath-hold Acquisition in FDG PET/CT in the Assessment of Lung nodules. Radiology. 2018;286(1):260–70. https://doi.org/10.1148/radiol.2017160534.
15. Cheng Z, Chen L, Wang X et al. Role of breath-hold lung PET in stage IA pulmonary adenocarcinoma. Insights Imaging. 2023;14(1):100. Published 2023 May 25. https://doi.org/10.1186/s13244-023-01446-1
16. Nagamachi S, Wakamatsu H, Kiyohara S, et al. Usefulness of a deep-inspiration breath-hold 18F-FDG PET/CT technique in diagnosing liver, bile duct, and pancreas tumors. Nucl Med Commun. 2009;30(5):326–32. https://doi.org/10.1097/MNM.0b013e3283298f78.

17. Nagamachi S, Wakamatsu H, Kiyohara S, et al. The reproducibility of deep-inspiration breath-hold (18)F-FDG PET/CT technique in diagnosing various cancers affected by respiratory motion. Ann Nucl Med. 2010;24(3):171–8. https://doi.org/10.1007/s12149-010-0352-3.
18. Torizuka T, Tanizaki Y, Kanno T, et al. Single 20-second acquisition of deep-inspiration breath-hold PET/CT: clinical feasibility for lung cancer. J Nucl Med. 2009;50(10):1579–84. https://doi.org/10.2967/jnumed.109.064246.
19. Karp JS, Surti S, Daube-Witherspoon ME, Muehllehner G. Benefit of time-of-flight in PET: experimental and clinical results. J Nucl Med. 2008;49(3):462–70. https://doi.org/10.2967/jnumed.107.044834.
20. Guiyu L, Wenhui M, Xiang L, et al. Performance evaluation of the uMI Panorama PET/CT system in accordance with the National Electrical Manufacturers Association NU 2-2018 Standard. J Nucl Med. 2024;65:1–8. https://doi.org/10.2967/jnumed.123.265929.
21. Hofland J, Kaltsas G, de Herder WW. Advances in the diagnosis and management of well-differentiated neuroendocrine neoplasms. Endocr Rev. 2020;41(2):371–403. https://doi.org/10.1210/endrev/bnz004.
22. Grey N, Silosky M, Lieu CH, Chin BB. Current status and future of targeted peptide receptor radionuclide positron emission tomography imaging and therapy of gastroenteropancreatic-neuroendocrine tumors. World J Gastroenterol. 2022;28(17):1768–80. https://doi.org/10.3748/wjg.v28.i17.1768.
23. Desai H, Borges-Neto S, Wong TZ. Molecular imaging and therapy for neuroendocrine tumors. Curr Treat Options Oncol. 2019;20(10):78. https://doi.org/10.1007/s11864-019-0678-6. Published 2019 Aug 29.
24. Hope TA, Allen-Auerbach M, Bodei L, et al. SNMMI Procedure Standard/EANM Practice Guideline for SSTR PET: imaging neuroendocrine tumors. J Nucl Med. 2023;64(2):204–10. https://doi.org/10.2967/jnumed.122.264860.
25. Adnan A, Basu S. Somatostatin receptor targeted PET-CT and its role in the management and theranostics of gastroenteropancreatic neuroendocrine neoplasms. Diagnostics (Basel). 2023;13(13):2154. https://doi.org/10.3390/diagnostics13132154. Published 2023 Jun 24.
26. Hou J, Long T, Yang N, et al. Biodistribution of 18F-AlF-NOTA-octreotide in different organs and characterization of Uptake in Neuroendocrine neoplasms. Mol Imaging Biol. 2021;23(6):827–35. https://doi.org/10.1007/s11307-021-01628-7.
27. Long T, Yang N, Zhou M, et al. Clinical application of 18F-AlF-NOTA-Octreotide PET/CT in Combination with 18F-FDG PET/CT for imaging neuroendocrine neoplasms. Clin Nucl Med. 2019;44(6):452–8. https://doi.org/10.1097/RLU.0000000000002578.
28. Leupe H, Ahenkorah S, Dekervel J, et al. 18F-Labeled somatostatin analogs as PET Tracers for the somatostatin receptor: ready for clinical use. J Nucl Med. 2023;64(6):835–41. https://doi.org/10.2967/jnumed.123.265622.
29. Liu M, Zhu W, Zhang Y, et al. A prospective evaluation of [18F]AlF-NOTA-LM3 in patients with well-differentiated neuroendocrine tumors: head-to-head comparison with 68Ga-DOTATATE. EANM'23 Abstract Book Congress Sep 9–13, 2023. Eur J Nucl Med Mol Imaging. 2023;50(Suppl 1):1–898. https://doi.org/10.1007/s00259-023-06333-x.
30. Liu M, Ren C, Zhang H, et al. Evaluation of the safety, biodistribution, dosimetry of [18F]AlF-NOTA-LM3 and head-to-head comparison with [68Ga]Ga-DOTATATE in patients with well-differentiated neuroendocrine tumors: an interim analysis of a prospective trial. Eur J Nucl Med Mol Imaging Published Online June. 2024;15. https://doi.org/10.1007/s00259-024-06790-y.
31. Sigfridsson J, Lindström E, Iyer V, et al. Prospective data-driven respiratory gating of [68Ga]Ga-DOTATOC PET/CT. EJNMMI Res. 2021;11(1):33. https://doi.org/10.1186/s13550-021-00775-w. Published 2021 Mar 31.

Publisher's Note